

CONFERENCES AND SYMPOSIA PACS numbers: 29.25.Bx, **79.60.–i**

Electron gun with a transmission photocathode for the Joint Institute for Nuclear Research photoinjector

N I Balalykin, V F Minashkin, M A Nozdrin, G D Shirkov, V V Zelenogorskii, E I Gacheva, A K Potemkin, J Huran

DOI: https://doi.org/10.3367/UFNe.2017.03.038145

Contents

Abstract. **Photocathode electron guns are key to the generation of high-quality electron bunches, which are currently the primary source of electrons for linear electron accelerators. The photogun test bench built at the Joint Institute for Nuclear Research (JINR) is currently being used to further develop the hollow (backside irradiated) photocathode concept. A major achievement was the replacement of the hollow photocathode by a technologically more feasible transmission photocathode made from a metal mesh that serves as a substrate for films of various photomaterials. A number of thin-film cathodes on quartz glass substrates are fabricated by photolithography. The vectorial photoeffect (related to the surface-normal component of the wave electric field) is observed and found to significantly affect the quantum efficiency. The dependence of the quantum efficiency of diamond-like carbon photocathodes on the manufacturing technology is investigated. The Rutherford backscattering and elastic recoil detection techniques are combined to carry out an elemental analysis of the films. An estimate of the emittance of a 400 pC electron beam is obtained using the cross-section method.**

N I Balalykin, V F Minashkin, M A Nozdrin, G D Shirkov Joint Institute for Nuclear Research,
ul. Joliot-Curie 6, 141980 Dubna, Moscow region, Russian Federation
E-mail: nozdrin@jinr.ru
V V Zelenogorskii, E I Gacheva, A K Potemkin Institute of Applied Physics, Russian Academy of Sciences,
ul. Ul'yanova 46, 603950 Nizhny Novgorod, Russian Federation
J Huran Institute of Electrical Engineering,
Dúbravská cesta 9, 84104 Bratislava, Slovak Republic

Received 30 March 2017
Uspekhi Fizicheskikh Nauk **187** (10) 1134 – 1141 (2017)
DOI: https://doi.org/10.3367/UFNr.2017.03.038145
Translated by E N Ragozin; edited by A M Semikhatov

Keywords: DC photoinjector, transmissive photocathode, vectorial photoeffect

1. Introduction

Photocathodes are important elements of modern electron accelerators. Despite the considerable progress achieved in this area, research is being actively pursued to develop new and optimize existing photoguns and photocathodes. A new concept of photocathode design was proposed at the Joint Institute for Nuclear Research (JINR): a backside-illuminated 'hollow' photocathode of a massive material made in the form of a disk with a cylindrical or conical opening at the center. The working cathode surface is the wall of the conical or cylindrical opening. The geometry of this cathode permits an increase in the opening wall quantum efficiency due to the vectorial photoeffect. Furthermore, the backside irradiation greatly simplifies alignment to the emitting surface and its laser cleaning after the initial installation of the cathode and during its maintenance.

During experimental investigations, the hollow photocathode was replaced with a 'transparent' one, which is a micrometer-size mesh structure. Two substrate types were used for making these photocathodes.

(1) A metal 40×40 μm cell mesh of copper or stainless steel wires 30 μm in diameter. An oxygen-free copper mesh itself can serve as the photocathode. A stainless steel mesh is a good substrate for thin-film photocathodes of metals and their compounds (Cu, TiN, NbC), as well as of semiconductors (diamond-like carbon, SiC).

(2) Optically polished 0.4 mm thick quartz glass 10×10 mm in transverse size.

As regards transparent photocathode production, the fundamental difference between these substrate types is that the former involve front-side laser irradiation with a varying angle of incidence (Fig. 1b), while the latter employ backside

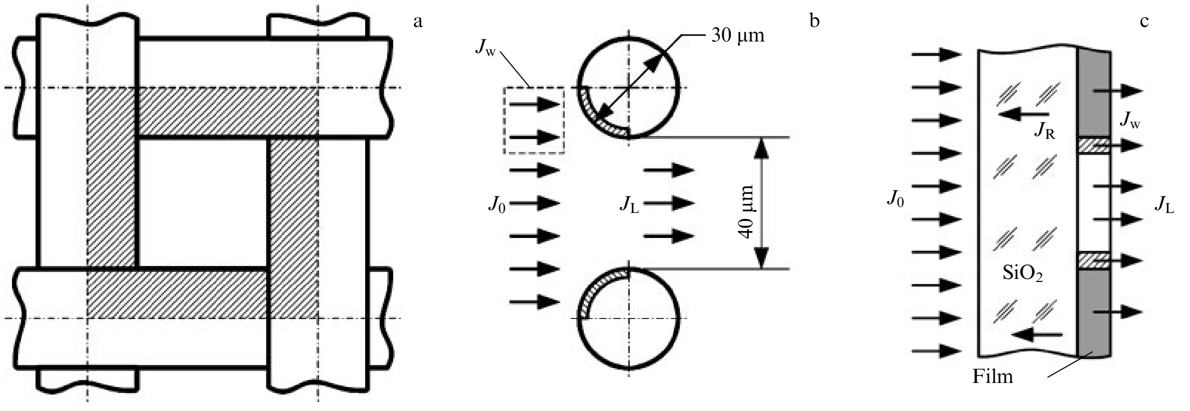

Figure 1. Cell of a transparent photocathode on a substrate (a, b) of metal mesh ((a) top and (b) side views) and (c) of quartz glass (side view). The shading indicates the working cell zone. J_0 — total flux, J_w — working flux, i.e., the photon flux capable of producing the photoeffect, J_L — transmission loss flux, J_R — reflection loss flux (the photon flux that does not participate in photoeffect production).

irradiation (Fig. 1c). It is precisely the second type of substrate that allows most amply inducing and harnessing the vectorial photoeffect.

2. Equipment

2.1 Photogun test bench

Photocathodes are investigated on a photogun test bench. It comprises a DC photogun with a maximum anode voltage of 30 keV, a laser driver, a focusing magnet, and various types of diagnostic equipment. The pressure in the path of the test bench is of the order of or lower than 10^{-8} Torr. The main laser driver in use is LS-2134 (JV LOTIS TII), which provides 15 mJ, 15 ns long pulses at a wavelength of 266 nm. Readers can familiarize themselves with detailed information on the test bench equipment and the lasers in use in Ref. [1].

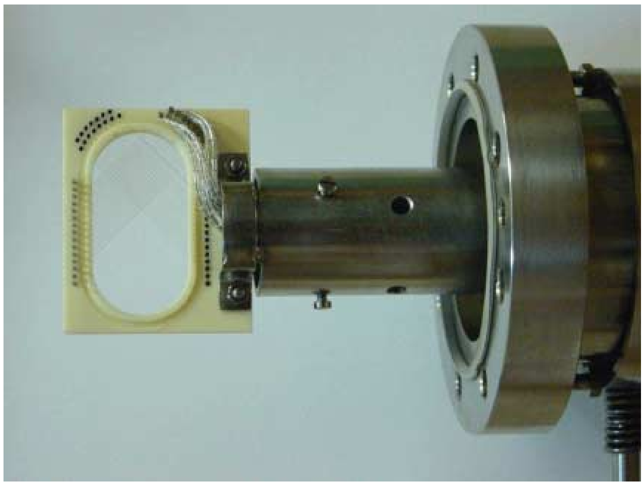

Figure 2. Wire electrode unit of an emittance measurement station.

2.2 Diagnostic equipment

In the experiments described below, the electron bunch charge was measured with a Faraday cup grounded with a matched cable via a measuring capacitor with a capacitance of 560 pF. The voltage across the capacitor was recorded with a 500 MHz oscilloscope. The relation between the extracted charge and the laser energy for a constant accelerating voltage was investigated. The quantum efficiency was calculated using the voltage across the capacitor measured for a low extracted charge: we used the portion of the charge–laser-energy dependence in which the effect of the spatial charge was weak and the dependence was linear. For photocathodes with a metal mesh substrate, the number of laser photons incident on the photocathode was measured with an Ophir Nova II energy/power meter with a PE25 pyroelectric sensor, taking the transmittance of the input window of the vacuum chamber and of the mesh cathode itself into account. For photocathodes with a quartz glass substrate, the number of photons was determined in the same way as for photocathodes of the first type, but a substantial portion of the radiation did not participate in the process in this case.

An AVT Prosilica GC1380 video camera with a Kowa LM50JCM lens combined with the AVINE code package developed at the DESY acceleration center in Zeuthen was used for video diagnostics of the laser beam, primarily on the virtual cathode. The diagnostic equipment is described at length in Ref. [2].

To estimate the electron beam emittance by the method of cross sections, a system of two z-coordinate-spaced stations with wire electrodes was used (two planes with 15 wires in each plane per station) (Fig. 2). The information was transmitted from the wires to a readout unit via coaxial cables and then to a PC via an RS-232 interface. The data received by the computer were processed and visualized: the charge distributions over the wires were plotted in the form of four one-dimensional and two two-dimensional histograms (Fig. 3).

2.3 Photoinjector test bench

The photogun test bench should develop into a full-scale photoinjector test bench designed for an energy up to 400 keV. The ultraviolet (UV) laser driver [3] intended for the test bench was developed by the Institute of Applied Physics, Russian Academy of Sciences (Nizhny Novgorod). Unlike the lasers used in the photogun test bench, the laser (Fig. 4) is not a single-pulse one but produces sequences (macropulses) of identical short pulses (micropulses), up to 8000 in a sequence. The macropulse repetition rate is equal to 10 Hz, the laser wavelength is equal to 262 nm, the micropulse duration is 8–10 ps, and the micropulse energy is 1.5 μJ.

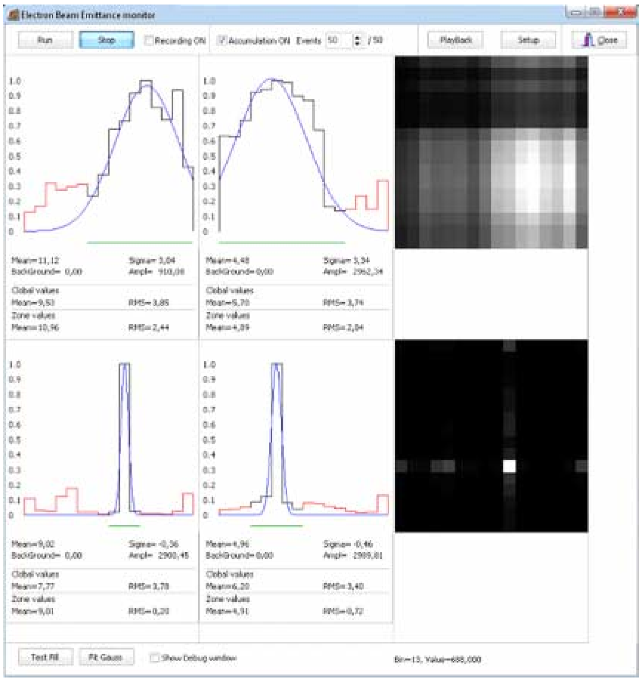

Figure 3. Window of the visualization program.

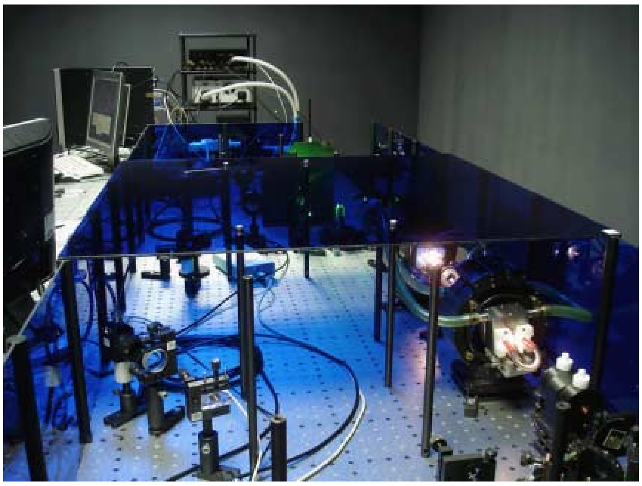

Figure 4. Laser driver in operation.

Measurements of the micropulse repetition rate of the master oscillator showed that it fluctuates in a very narrow frequency interval of about 10 Hz (design value: 50–100 Hz) and is tunable in a broad frequency range of ± 1.3 kHz. After a half-hour warm-up, the average micropulse repetition rate varied only slightly and only when there was an ambient temperature variation. The uniqueness of the driver is in the set of its parameters, which are uncharacteristic of laser engineering: none of the parameters being a record, their optimal combination permits stating that the system as a whole is highly competitive on the market of laser drivers intended for accelerators.

The laser radiation is delivered to the photocathode using an optical transport line, which images a round pinhole 5 mm in diameter onto the photocathode with a demagnification of 1:5 (Fig. 5). The transport line also permits rotating the linear radiation polarization at an arbitrary angle using a half-wave plate and monitoring the transverse beam distribution, the macropulse shape, and the UV radiation power in front of the photocathode.

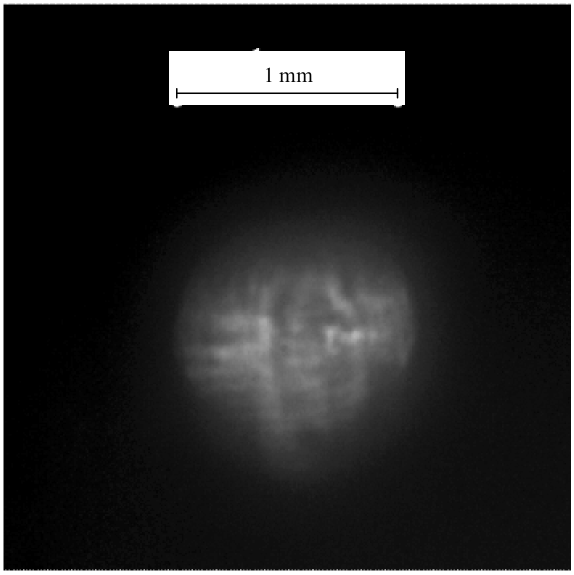

Figure 5. Laser beam in the photocathode plane.

3. Results

3.1 Transparent GaAs photocathode

The photocathode was made of crystalline gallium arsenide by Freon-12 (CCl_2F_2) plasma etching for a power of 150 W, a pressure of 18 Pa, and a CCl_2F_2 flux of 30 standard cubic centimeters per minute (sccm). The resist mask, which was patterned by e-beam lithography, was a plate with square openings with a side of 200 μm and the same spacing of the square openings in both directions. A 200 nm thick nickel layer was deposited by evaporation on the mask and, after removal of the resist and the excess nickel, a nickel mask for etching was obtained. The CCl_2F_2 plasma etching lasted for 8 h, after which the nickel mask was removed by etching in an H_3PO_4:H_2O_2:$10H_2O$ solution at room temperature. The cathode fabrication procedure and the cathode surface are shown schematically in Fig. 6.

The quantum efficiency was investigated for an anode voltage of 12 keV and the laser beam spot size $\leqslant 5$ mm. The highest extracted charge amounted to 2.2 nC, which corresponded to a quantum efficiency $\geqslant 1 \times 10^{-5}$. Because we primarily investigated the technical feasibility of making a transparent photocathode of gallium arsenide, a low-quality sample was used, which led to a low quantum efficiency.

3.2 Diamond-like carbon film photocathodes on a metal mesh

Diamond-like carbon (DLC) films were deposited on silicon substrates and on stainless steel substrate cathodes, which had the form of a wire mesh 30 μm in diameter with a 40×40 μm cell size, by reactive magnetron sputtering (RMS) of a carbon target in $Ar + D_2$ and $Ar + H_2$ gas mixtures, as well as by plasma-enhanced chemical vapor deposition (PECVD) of $CH_4 + D_2 + Ar$ and $CH_4 + H_2 + Ar$ mixtures. In the course of deposition by the above techniques, standard procedures and regimes determined by accumulated technological expertise were observed. Therefore, we investi-

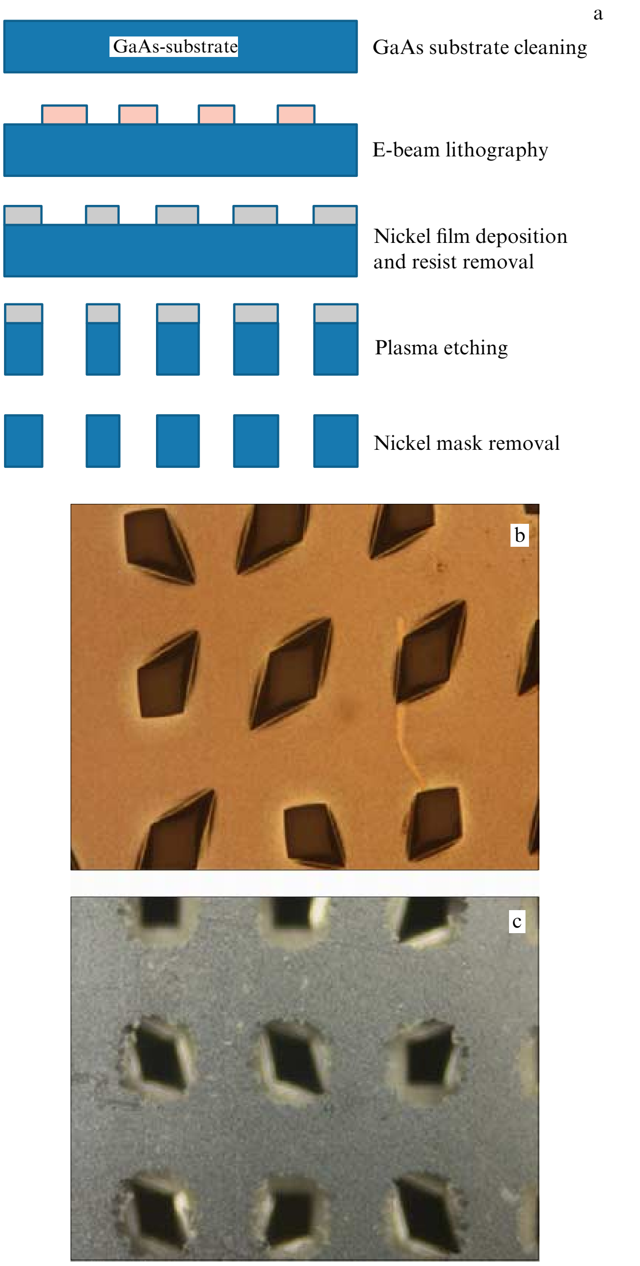

Figure 6. (a) Schematic of GaAs photocathode fabrication. (b) Top and (c) bottom photocathode surface views.

gated four cathode samples: those made by RMS with hydrogen (MH) and deuterium (MD) gas mixtures and those made by PECVD with the same gases (PH and PD).

An elemental analysis of the films was simultaneously performed by the Rutherford backscattering spectroscopy (RBS) and elastic recoil detection (ERD) techniques [4]. Raman light scattering was used in the analysis of the sp2/sp3 carbon phase ratio (graphite phase/diamond phase) in the films. The investigation was carried out with a Thermo Scientific DXR Raman Microscope with a 532 nm laser beam. The graphite and diamond peaks were approximated with Gaussians and the intensity was calculated as the peak area.

The composition analysis showed that the films are made of carbon, hydrogen, deuterium, and a small amount of oxygen. Table 1 shows the percentage of these elements, as well as the diamond-to-graphite ratios $I(\mathrm{D})/I(\mathrm{G})$ in the four

Table 1. Percentage of elements and $I(\mathrm{D})/I(\mathrm{G})$ ratio in different DLC film samples.

Sample \ Element	C	H	D	O	$I(\mathrm{D})/I(\mathrm{G})$
PD	61	26	12	1–2	1.443
PH	71	27	0	1–2	1.133
MD	59	5	33	2–3	1.723
MH	64	33	0	2–3	1.473

samples listed above. More detailed information is available in Ref. [5].

To determine the quantum efficiency from diamond-like films, we investigated the transparent cathode of a stainless mesh substrate. Figure 7 shows the dependence of the bunch charge on the laser energy for different accelerating voltages. For an accelerating voltage of 3 kV, the bunch charge increases from 0 to 411 pC with the laser energy increasing from 0 to 3 mJ. With a further increase in laser energy to 4.8 mJ, the charge hardly changes and amounts to 413 pc. Therefore, the photogun operates in the space charge saturation mode for a laser energy above 3 mJ. A similar picture is observed for an accelerating voltage of 5 kV: the saturation mode sets in for the laser energy greater than 3 mJ (the charge 581 pC) and changes only slightly, ranging up to 615 pC with increasing the laser energy to 4.8 mJ. The picture changes when the voltage is increased from 6 to 11 kV: the charge tends to increase appreciably with an increase in the accelerating voltage. The reason for this is unclear to us. We can only hypothesize, taking the geometrical dimensions of the mesh substrate into account (the wire radius: 15 μm), that the field emission becomes essential along with the photoemission. The quantum efficiency of the stainless mesh cathode was equal to 1.1×10^{-6}.

The cathodes with deposited films were investigated for an anode voltage of 10 kV. Figure 8 shows the dependence of the bunch charge on the laser energy for different cathode samples. Given for comparison is a similar dependence for the stainless steel mesh cathode without any film. Increasing the laser energy results in an increase in the number of photons participating in photoemission, which in turn leads to an increase in the number of photoelectrons. The quantum efficiency of the respective MD, MH, PD, and PH samples was equal to 3.2×10^{-6}, 2.4×10^{-6}, 2.6×10^{-6}, and 2.2×10^{-6}. Figure 9 shows the quantum efficiency and

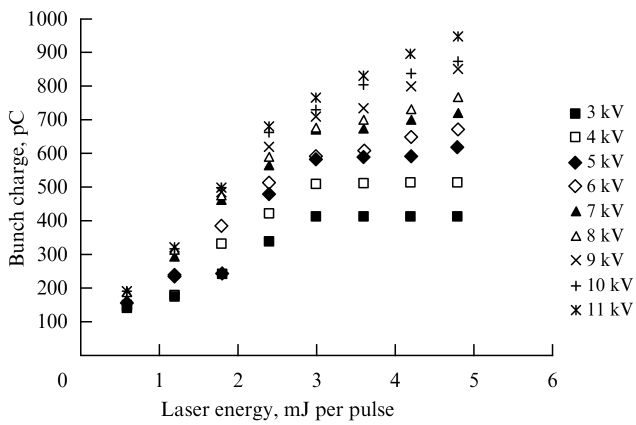

Figure 7. Bunch charge versus to the laser energy for different anode voltages.

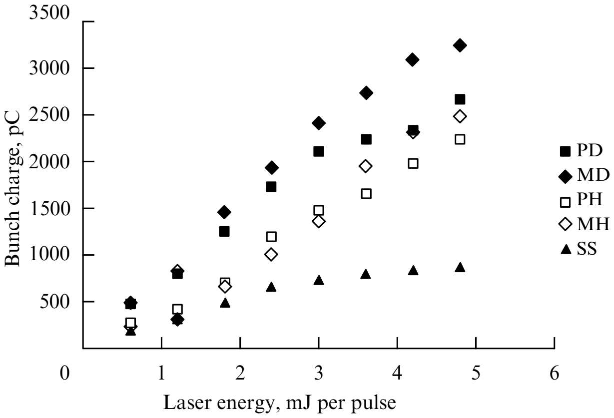

Figure 8. Bunch charge versus to the laser energy for different cathode samples, including the uncoated stainless steel mesh (SS).

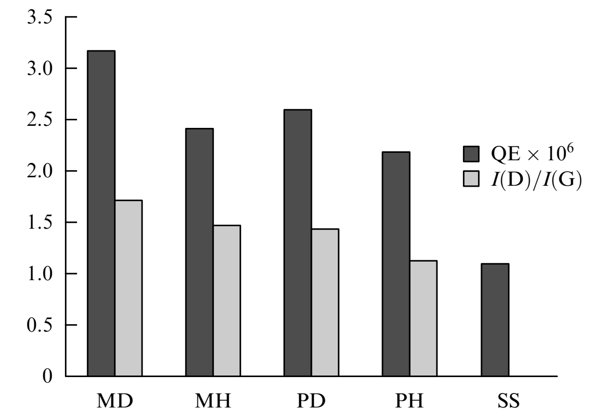

Figure 9. Quantum efficiency (QE) and the $I(\mathrm{D})/I(\mathrm{G})$ ratio for different cathodes.

the $I(\mathrm{D})/I(\mathrm{G})$ ratio for different samples. As we can see, the higher the $I(\mathrm{D})/I(\mathrm{G})$ ratio is, the higher the quantum efficiency.

3.3 Nitrogen-doped diamond-like film photocathodes on quartz glass substrates

Nitrogen-doped diamond-like carbon (DLC(N)) films were deposited on substrates of silicon, stainless steel meshes (MS samples), and quartz glass coated with a 5 nm thick chromium film to improve the adhesion properties by the RMS technique (MQ samples). The magnetron target was a high-purity graphite disk 76.2 mm in diameter. For an inert gas, high-purity argon was used, and a 90% nitrogen and 10% hydrogen mixture was employed as a reactive gas. The flow rate of argon was equal to 30 sccm for all samples. The (90% N_2 + 10% H_2)-mixture flow rate was 2, 4, and 8 sccm for the respective MQ2, MQ3, and MQ4 samples. For the MQ1 sample, the DLC film was deposited without a reactive gas. The working pressure was equal to 0.6 Pa; the input magnetron power comprised an AC (200 W, 13.56 MHz) component and a DC (550 V, 150 mA) one. The substrate holder was kept at a voltage of -150 V, its temperature being 100 °C. The film thickness was equal to 200–250 nm on the silicon and metal mesh substrates and about 25 nm on quartz glass. The DLC films were deposited on both sides of the mesh under similar conditions. The films on

Table 2. Percentage of elements the and $I(\mathrm{D})/I(\mathrm{G})$ ratios in different DLC(N) film samples

Sample \ Element	C	N	H	O	$I(\mathrm{D})/I(\mathrm{G})$
MS1	90	1 – 2	7	1 – 2	1.49
MS2	70	15	14	1 – 2	0.45
MS3	64	21	14	1 – 2	0.78
MS4	61	23	15	1 – 2	1.49

silicon substrates were used to investigate the composition of different samples. To provide charge inleakage, an aluminum mesh was deposited on the DLC films on quartz glass using lift-off lithography. Figure 10 shows the processing sequence for the fabrication of the cathode with a DLC film on quartz glass and a photograph of such a cathode.

To investigate the vectorial photoeffect, the cathodes on quartz glass were irradiated by high-intensity laser pulses (3–4 pulses with an intensity of 5 MW cm^{-2}) to produce a micrometer-size perforation in chromium and DLC films.

The method used for investigating the film composition was similar to the method described in Section 3.2. Table 2 shows the composition of the MS1–MS4 samples and the diamond/graphite phase ratio. The investigation of the film composition is described in greater detail in Ref. [6].

The cathodes were investigated at an anode voltage of 20 kV. Figure 11a shows the relation between the bunch charge and the laser energy for the MQ1–MQ4 samples after micrometer-size perforation. The charge extracted from the MS1–MS4 samples was approximately three times smaller. Figure 11b shows the quantum efficiency of all samples under investigation. We can see that the quantum efficiency becomes higher with increasing the nitrogen density in the film. Also observed is a significant increase in the quantum efficiency after the MQ photodiode perforation due to the vectorial photoeffect.

3.4 Phosphorus-doped silicon–carbide photocathodes on quartz glass substrates

Phosphorus-doped silicon–carbide (SiC(P)) films were deposited on a silicon substrate for the investigation of their composition and on double-sided polished quartz glass (10 × 10 mm) for making transparent photocathodes by the PECVD technique. The technical features of the preparation of different samples are collected in Table 3.

To form the perforation in the film, we used dry etching in an SF_6 plasma. The etching was carried out on an Oxford Instruments Plasmalab System 100 ICP-RIE instrument

Table 3. Technological data of the preparation of different SiC(P)-film samples.

Sample	Gas flow rate, sccm				T, °C	P, Pa	W, W
	CH_4	SiH_4	H_2	PH_3			
QP1	20	5	100	10	350	100	100
QP2				30			
QP3			—	20		70	
QP4				50			
QP5				100			

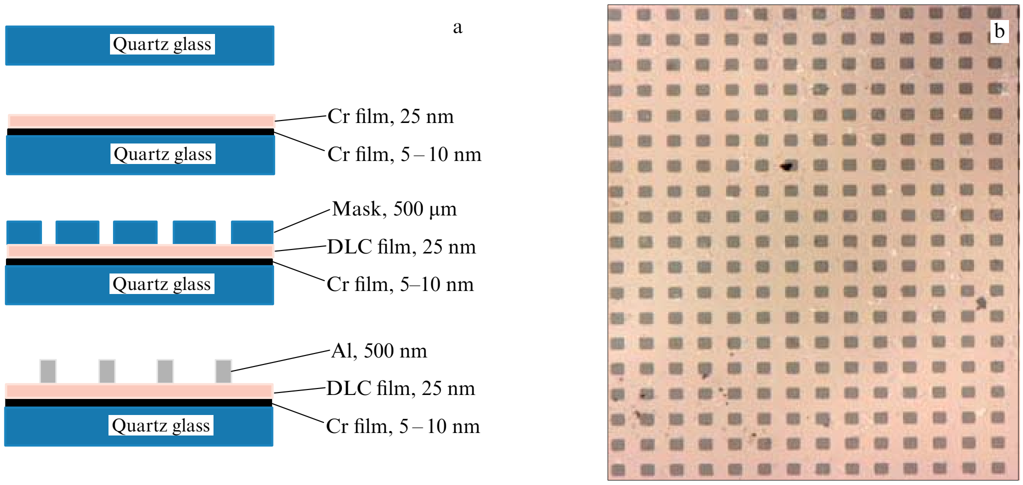

Figure 10. (a) Technology of transparent photocathode fabrication on quartz glass coated with a DLC film. (b) External appearance of this cathode.

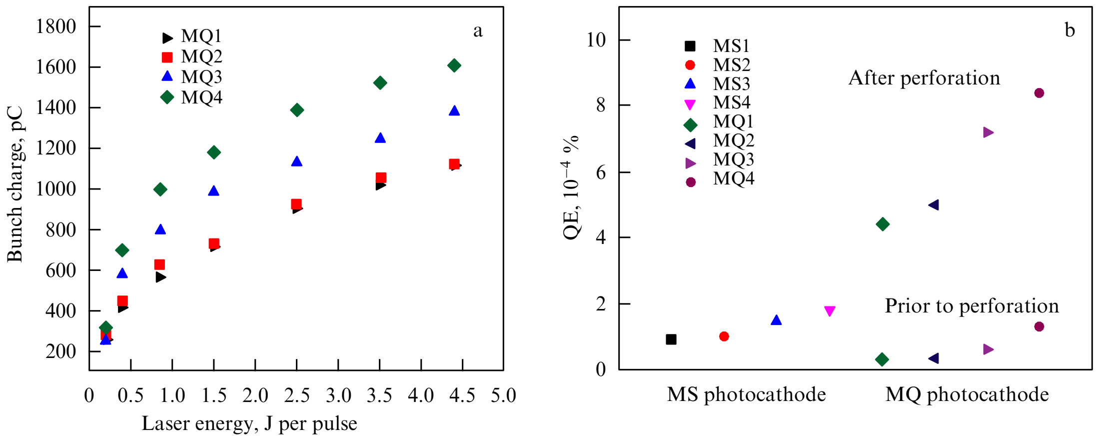

Figure 11. (a) Dependence of the bunch charge on the laser energy. (b) Quantum efficiency of the MS and MQ (prior to and after perforation) samples.

with the following parameters of the process: SF_6 flow rate 20 sccm; power and frequency of inductively coupled plasma source 400 W and 13.56 MHz; pressure 10 mTorr; and the electrode temperature 20 °C. The etching time was 4–6 min, depending on the film thickness. For a mask, an aluminum mesh deposited by photolithography and the lift-off technique was used, which was removed after etching. Deposited next, also by the lift-off technique, was a contact aluminum mesh. The processing sequence for the transparent cathode fabrication and the appearance of the resultant mesh are shown in Fig. 12. The cathodes thus made were SiC(P) meshes with square 20 × 20 μm cells spaced at 20 μm.

The method of investigating the film composition is similar to that described in Section 3.2. The results of investigations are given in Table 4. Apart from the indicated elements, all films contained small amounts of oxygen and nitrogen due to adsorption from chamber walls during the deposition.

The quantum efficiency of different samples of phosphorus-doped silicon-carbide photocathodes is shown in Fig. 13. We can see that the quantum efficiency increases with increasing the phosphorus content up to 10 atomic percent and decreases sharply upon a further increase in the phosphorus content. The reason can lie with a significant change in the cathode properties, with the result that the energy of electron affinity begins to increase.

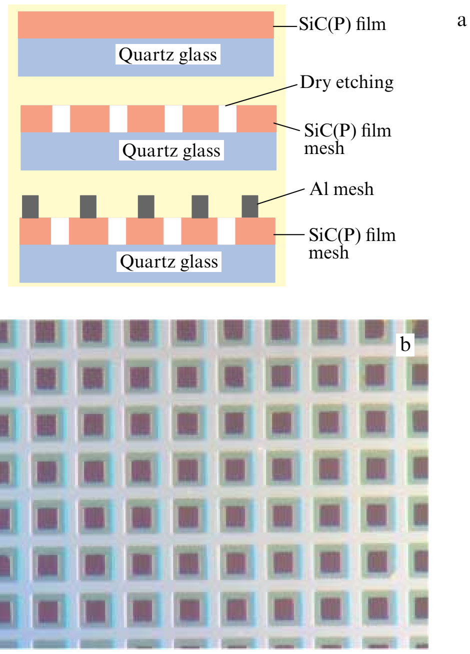

Figure 12. (a) Technology of fabricating a transparent photocathode on quartz glass coated with an SiC(P) film and (b) the external appearance of such a cathode.

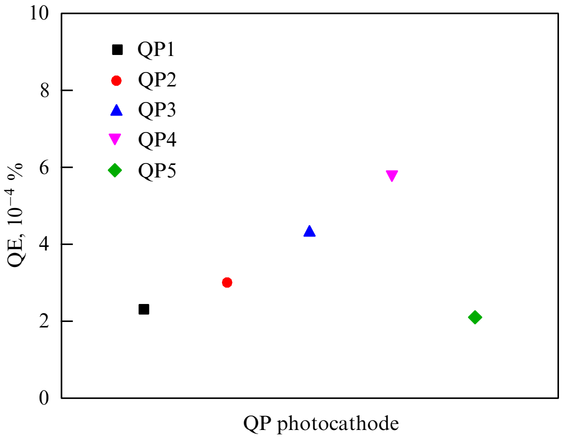

Figure 13. Quantum efficiency of various SiC(P) cathode samples.

Table 4. Atomic percentage of elements in various SiC(P) film samples

Sample \ Element	Si	C	H	P
QP1	35	32	32	1
QP2	35	32	31	2
QP3	34	30	31	5
QP4	33	29	28	10
QP5	31	26	28	15

3.5 Other photocathode samples

Apart from the cathodes described above, investigations were performed of cathodes of both versions (stainless steel mesh and quartz glass) made of titanium nitride, niobium carbide, and phosphorus-doped silicon carbide, as well as of a copper mesh cathode without a coating. The highest extracted charge and the quantum efficiency of the copper mesh cathode were respectively equal to 840 pC and 9.8×10^{-6}.

In general, the highest quantum efficiency of the cathodes on quartz glass substrates was 2–5 times higher than the highest quantum efficiency of the cathodes on metal mesh substrates. Specifically, for the TiN cathode on a stainless steel mesh, the highest quantum efficiency was 1.8×10^{-6}, while its efficiency on quartz glass was 5.0×10^{-6} (extracted charge 410 pC). The corresponding figures for NbC were 1.5×10^{-6} and 7.2×10^{-6} (charge 570 pC). For the SiC(P) cathode on quartz glass, the highest extracted charge and the quantum efficiency were 800 pC and 9.0×10^{-6}.

3.6 Photocathode efficiency

We can see that the measured quantum efficiency is appreciably lower than for ‘traditional’ frontside-illuminated photocathodes. This is attributable to the method of estimating the number of photons incident on a cathode. In our case, this number is taken to be equal to the number of photons that are not transmitted through the cathode, which accounts for about 50% of their total number in the case of a hollow cathode and for 75% in the case of a transparent one. However, in reality, the photoeffect can be produced only by those photons that, conversely, pass through the cathode, namely, the photons that pass through almost the entire film and knock electrons out of its rear part as well as those that pass in the immediate vicinity of the walls of a mesh cell (within a distance of 20 nm) (Fig. 14). For the 30 × 30 μm

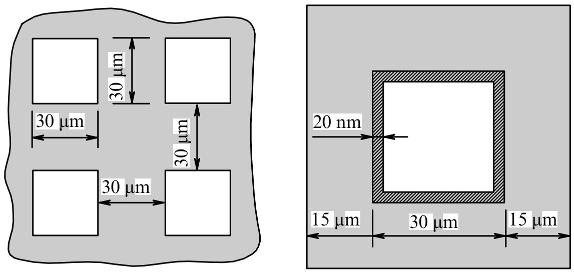

Figure 14. Schematic of the working zone of a transparent photocathode.

cell size (the case in point is a perforated film on quartz glass; in the case of a wire mesh, the contribution from the vectorial effect is considerably smaller due to the curvature of the cell surface), the area of this 20 nm zone is equal to about 1.2 μm^2, while the area of absorption zone is much greater, 2700 μm^2. From a comparison of these areas, we can assume a 2250 fold decrease in the photoeffect magnitude (by more than three orders of magnitude). However, this rough prediction is underestimated (in particular, because it does not include the contribution from photons that passed through the film and knocked photoelectrons out of its rear part), and a realistic estimate of the number of electrons capable of producing the photoeffect is extremely hard to make.

The thickness of the films deposited on the metal mesh is determined taking the technological requirements into account and is not bounded from below, usually amounting to 100–150 nm. In the case of film photocathodes on quartz glass, to maximize the efficiency, the film has to be much thinner than the optical skin depth. For instance, the calculated depth of the skin layer in copper for 266 nm radiation is about 20 nm and the film thickness should not exceed 4–5 nm. The preparation and investigation of photocathodes based on the perforated films of such a thickness is among the main lines of our future research.

3.7 Transverse emittance

The transverse emittance of an electron beam from a copper mesh cathode was estimated experimentally. Figure 15 shows the dependence of the normalized transverse emittance on the bunch charge for charges ranging from 5 to 400 pC. A further decrease in the emittance is anticipated with improvements in film surface quality (smoothness).

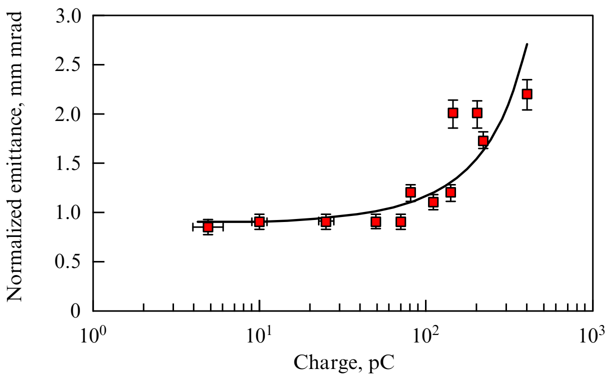

Figure 15. Dependence of the transverse emittance on the bunch charge.

4. Conclusions

We have investigated transparent photocathodes in the form of a thin film on substrates of micrometer-size metal mesh and quartz glass. The highest quantum efficiency of a film-free copper mesh cathode was 9.8×10^{-6}, of a cathode with a metal compound (NbC), 7.2×10^{-6}, and of semiconductor cathodes, 8.4×10^{-6} (DLC(N)) and 9.0×10^{-6} (SiC(P)) (all on quartz glass substrates). The use of the vectorial photoeffect was shown to hold much promise.

The main lines of further research involve improving the cathode efficiency by fabricating films no thicker than 4–5 nm and using lasers with wavelengths shorter than 200 nm.

References

1. Balalykin N I et al. *Phys. Part. Nucl. Lett.* **13** 897 (2016); *Pis'ma Fiz. Elem. Chast. At. Yad.* **13** 1398 (2016)
2. Nozdrin M A et al., JINR Commun. R9-2016-6 (Dubna: JINR, 2016)
3. Gacheva E I et al. *IEEE J. Quantum Electron.* **50** 522 (2014)
4. Kobzev A P et al. *Vacuum* **83** S124 (2009); in *Proc. of the Seventh Intern. Conf. on Ion Implantation and Other Applications of Ions and Electrons, ION 2008, 16 – 19 June 2008, Kazimierz Dolny, Poland*
5. Balalykin N I et al., in *2nd Intern. Conf. on Emission Electronics, Saint-Petersburg, Russia, 30 June – 4 July 2014, ICEE 2014* (Piscataway, NJ: IEEE, 2014) p. 1
6. Balalykin N I et al. *J. Phys. Conf. Ser.* **700** 012050 (2016)